



Contents lists available at ScienceDirect

Journal of Quantitative Spectroscopy & Radiative Transfer

journal homepage: www.elsevier.com/locate/jqsrt

Stratospheric and mesospheric H₂O and CH₄ trends from the ACE satellite mission

Anton M. Fernando^{a,*}, Peter F. Bernath^{a,b,c}, Christopher D. Boone^c^aOld Dominion University, Department of Physics, Norfolk, VA 23529, USA^bOld Dominion University, Department of Chemistry and Biochemistry, Norfolk, VA 23529, USA^cDepartment of Chemistry, University of Waterloo, Waterloo, Ontario, Canada

ARTICLE INFO

Article history:

Received 17 June 2020

Revised 17 August 2020

Accepted 17 August 2020

Available online 18 August 2020

Keywords:

Infrared remote sensing

CH₄ trendsH₂O trends

Atmospheric spectroscopy

ABSTRACT

The Atmospheric Chemistry Experiment (ACE) Fourier transform spectrometer (FTS) has been measuring water vapor and methane in the stratosphere and mesosphere from low Earth orbit since 2004. Recently, substantial increases in water vapor in the upper atmosphere were observed with the MLS and SABER satellite instruments. The main source of water vapor in the upper atmosphere is methane oxidation. ACE-FTS data show substantial water and methane increases, and confirm that the methane increases are too small to explain the water increases. Therefore, changes in the transport of water across the tropical tropopause layer and in atmospheric dynamics are responsible for the positive water trends.

© 2020 Elsevier Ltd. All rights reserved.

1. Introduction

Water in the stratosphere and mesosphere plays several important roles. In the stratosphere, water vapor is a climate active gas that cools the stratosphere and warms the surface [1]. In fact, stratospheric water vapor is calculated [2] to have a positive feedback effect in which increasing stratospheric water increases tropospheric temperatures, which in turn increase the amount of stratospheric water.

Water vapor is the main source of HO_x (H, OH, and HO₂), which destroys stratospheric ozone in the catalytic HO_x cycle [3]. Type 2 polar stratospheric clouds (PSCs) are composed of water ice, and liquid water is a component of Type 1b PSCs (supercooled nitric and sulfuric acid droplets) that lead to ozone destruction during polar spring [3]. In the mesosphere, water vapor freezes in the cold mesopause region around the time of the summer solstice to form polar mesospheric clouds (PMCs), e.g., Jones et al. [4]. The increasing occurrence of PMCs has been attributed to climate change, in particular to an increase in water vapor rather than a decrease in temperature although a decrease in mesopause temperatures has also been reported very recently [5,6].

The sources of water vapor in the stratosphere and mesosphere are from transport across the tropical tropopause layer which acts as a cold trap to dehydrate the ascending air as well as from the oxidation of CH₄. CH₄ originates from a wide variety of surface

sources and has an atmospheric lifetime of about 10 years. Like H₂O, it enters the stratosphere through the tropical tropopause, and is redistributed by the Brewer-Dobson circulation. CH₄ is oxidized by OH to make CH₃ and H₂O, then H₂CO and finally forms a second H₂O molecule and CO₂ [7]. The sum of the H₂O volume mixing ratio (VMR) and twice the CH₄ VMR is therefore approximately conserved in the stratosphere and has been termed “potential water” [8]. In the mesosphere, H₂O is lost by UV photolysis and water is also occasionally lost in the lower polar stratosphere by sedimentation of large PSCs (“dehydration”).

Trends in stratospheric and mesospheric water abundance are of interest because of their climate and chemical impact. Very recently, water vapor trends in the stratosphere and mesosphere were determined using the SABER (Sounding of the Atmosphere using Broadband Emission Radiometry) instrument on the TIMED (Thermosphere Ionosphere Mesosphere Energetics Dynamics) satellite and the MLS (Microwave Limb Sounder) instrument on Aura [9]. Yue et al. [9] found a positive trend at nearly all altitudes from 2002 to 2018. This water trend was larger than the surface trend of methane, but stratospheric methane observations were not included in their analysis. Noël et al. [10] studied methane and water trends in the stratosphere using the solar occultation measurements of the SCIAMACHY instrument on ENVISAT from 2002 to 2012 (when ENVISAT failed). A positive water trend was found in the lower stratosphere [10], which changes sign above about 30 km. Note that SCIAMACHY used the weak overtone water vapor band at 940 nm in their retrieval.

* Corresponding author.

E-mail address: afern018@odu.edu (A.M. Fernando).

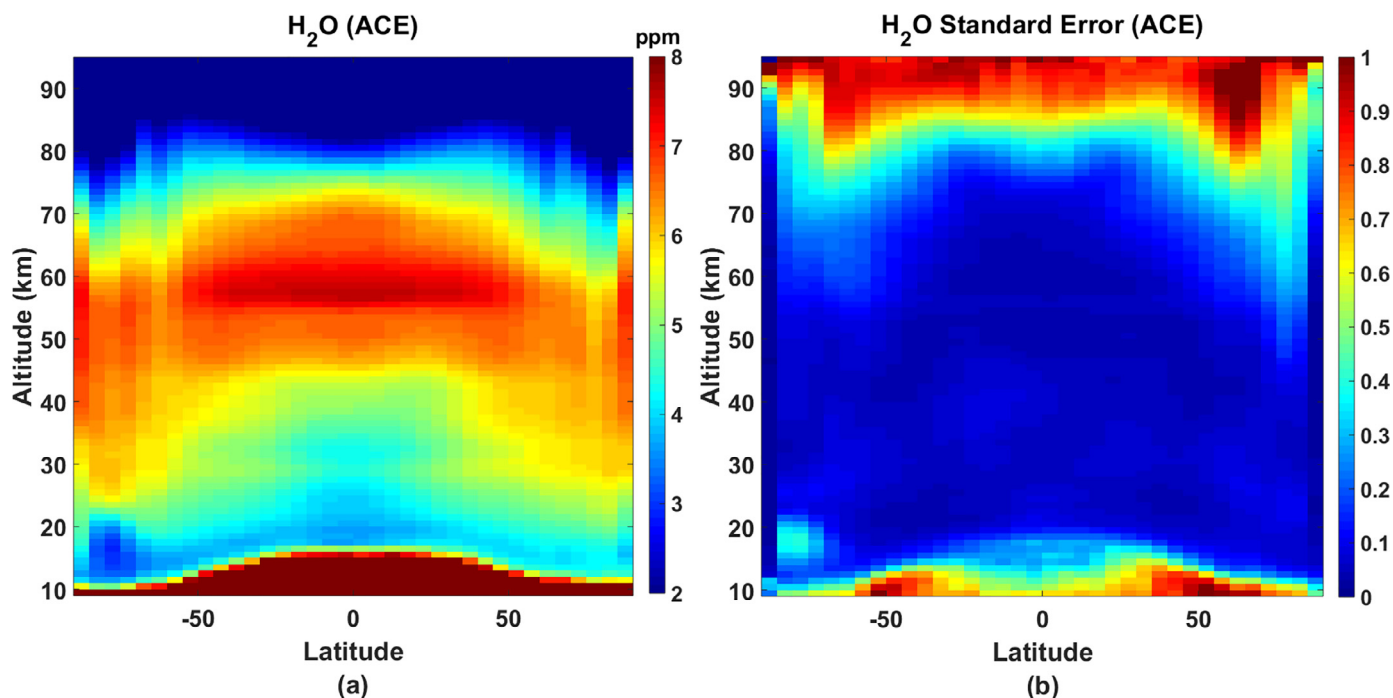


Fig. 1. ACE-FTS H₂O a) average altitude-latitude distribution and b) relative standard error distribution.

The Atmospheric Chemistry Experiment Fourier transform spectrometer (ACE-FTS) [11] has been measuring methane and water vapor by solar occultation since February 2004. As presented below, stratospheric and mesospheric trends are available for 2004 to the present for water, methane and potential water.

2. Observations and retrievals

ACE (Atmospheric Chemistry Experiment) is a satellite that has been in low-Earth orbit (650 km altitude, 74° inclination) since August, 2003. The ACE Fourier Transform Spectrometer (ACE-FTS) is the primary instrument that makes measurements of atmospheric molecules and their isotopologues by recording infrared spectra using the solar occultation method. Additionally, ACE-FTS provides aerosol extinction, from two filtered imagers, and temperature and pressure profiles. ACE-FTS covers the spectral region 750–4400 cm⁻¹ at high resolution (0.02 cm⁻¹) with a signal-to-noise ratio ranging from 100:1 up to ~ 400:1. Volume mixing ratio (VMR) profiles of H₂O from about 5 km to 95 km and VMR profiles of CH₄ from about 5 km to 75 km are provided on a 1 km vertical grid. The vertical resolution of ACE-FTS varies but is typically about 3 km. For this study, ACE-FTS version 4.0 is used for the time period 2004 (March) to 2020 (February) [12]. The linelist for ACE-FTS version 4.0 is based on spectroscopic parameters from HITRAN 2016 [13].

3. Results and discussion

ACE-FTS v4.0 data for H₂O from 10 km to 95 km and for CH₄ from 10 km - 75 km were used in our analysis. The altitude profiles of H₂O and CH₄ VMRs were filtered to remove outliers. All large and small values were removed from the data for each altitude and values more than 6 standard deviations away from the mission average were also removed. This data filtering process was run twice. In order to calculate the combined H₂O and CH₄ (potential water) linear trends, individual ACE-FTS VMR values were added using the equation $PW = \text{VMR H}_2\text{O} + 2 \times \text{VMR CH}_4$ to calculate potential water (PW) profiles.

Figs. 1 and 2 represent the mission average altitude-latitude distributions and the relative standard error profiles of H₂O and CH₄ VMRs on a 5° latitude and 1 km altitude grid, covering all latitudes from 2004 (March) to 2020 (only January and February data were used for 2020). The relative standard error profiles of H₂O and CH₄ (Fig. 1b and 2b) were calculated taking the ratio between the standard deviation and the average in each altitude-latitude bin. Fig. 3 represents the mission average altitude-latitude distributions and the relative standard error profiles of potential water VMRs.

ACE-FTS H₂O altitude-latitude VMR distribution (Fig. 1a) shows relative standard errors less than 20% between the altitudes 15.5 km and 74.5 km, and 70% outside (Fig. 1b). H₂O VMRs have values around 3.5 - 4.5 ppm between the altitudes 14.5 km - 44.5 km, and 6.5 - 7.5 ppm between the altitudes 44.5 km - 69.5 km in the latitude region 50°S - 50°N.

ACE-FTS CH₄ altitude-latitude VMR distribution (Fig. 2a) shows relative standard errors ~ 50% between the altitudes 21.5 km and 74.5 km in the latitude regions 50°S - 90°S and 50°N - 90°N near the poles, and less than 20% otherwise (Fig. 2b). The potential water altitude-latitude VMR distribution (Fig. 3a) shows relative standard errors ~ 20% in general (Fig. 3b) and approximately constant VMRs ~ 7 ppm in all the altitude-latitude bins (except in polar regions above 60 km and in the south pole between 10 - 20 km).

Figs. 4–7 represent the comparison of ACE-FTS H₂O VMR quarterly time series calculated for the latitude bins 55°N - 55°N and MLS and SABER global (55°N - 55°N) bimonthly running mean H₂O VMR time series for the altitudes ~ 29 km, ~ 49 km, ~ 63 km and ~ 82 km, for comparison with data presented by Yue et al. [9]. A fitted annual cycle and a semi-annual cycle were removed from ACE H₂O time series and local time variations were removed from MLS and SABER time series [9]. One standard deviation statistical errors on ACE data are indicated by pink shading in Figs. 4–7. Generally, MLS and SABER time series are in good agreement except at ~ 49 km [9]. At ~ 28 km VMRs of ACE-FTS time series are ~ 0.4 ppm higher than the VMRs of MLS and SABER time series. At ~ 49 km ACE-FTS time series is ~ 0.6 ppm lower than the MLS time series and ~ 1 ppm is lower than SABER time series. At

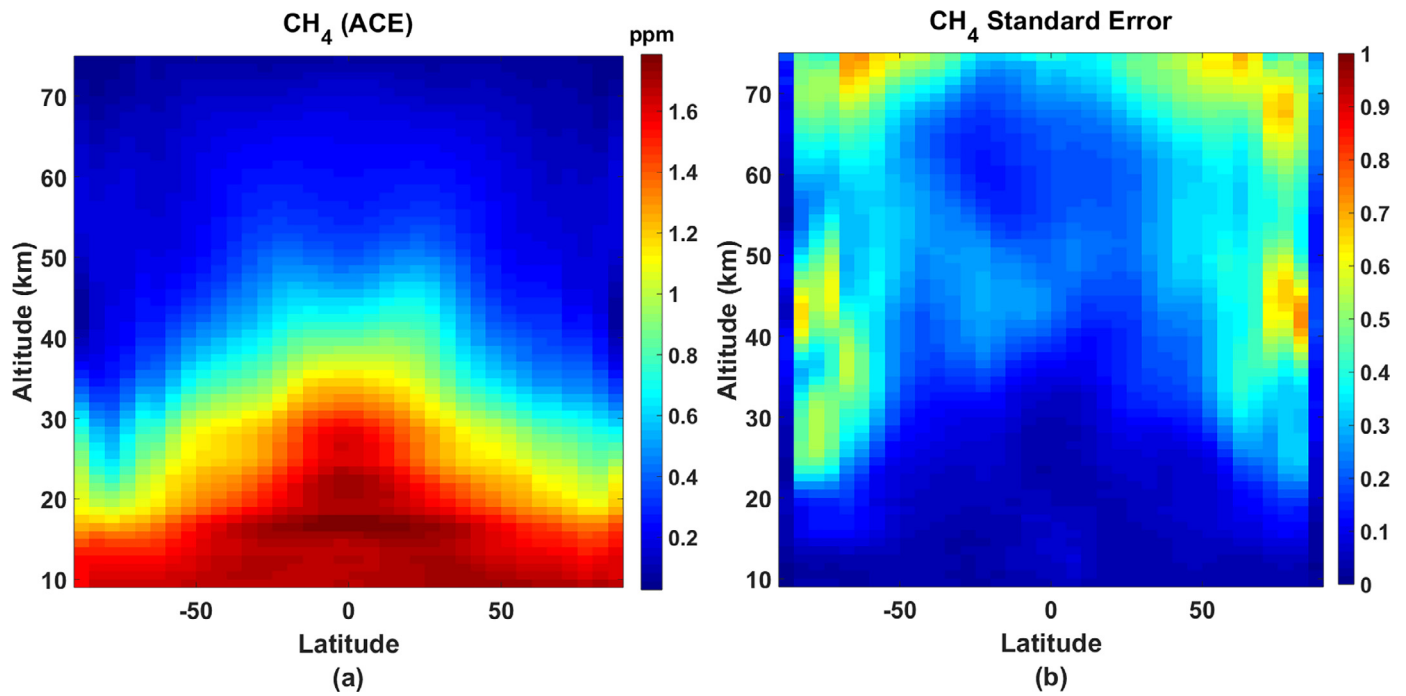


Fig. 2. ACE-FTS CH₄ a) average altitude-latitude distribution and b) relative standard error distribution.

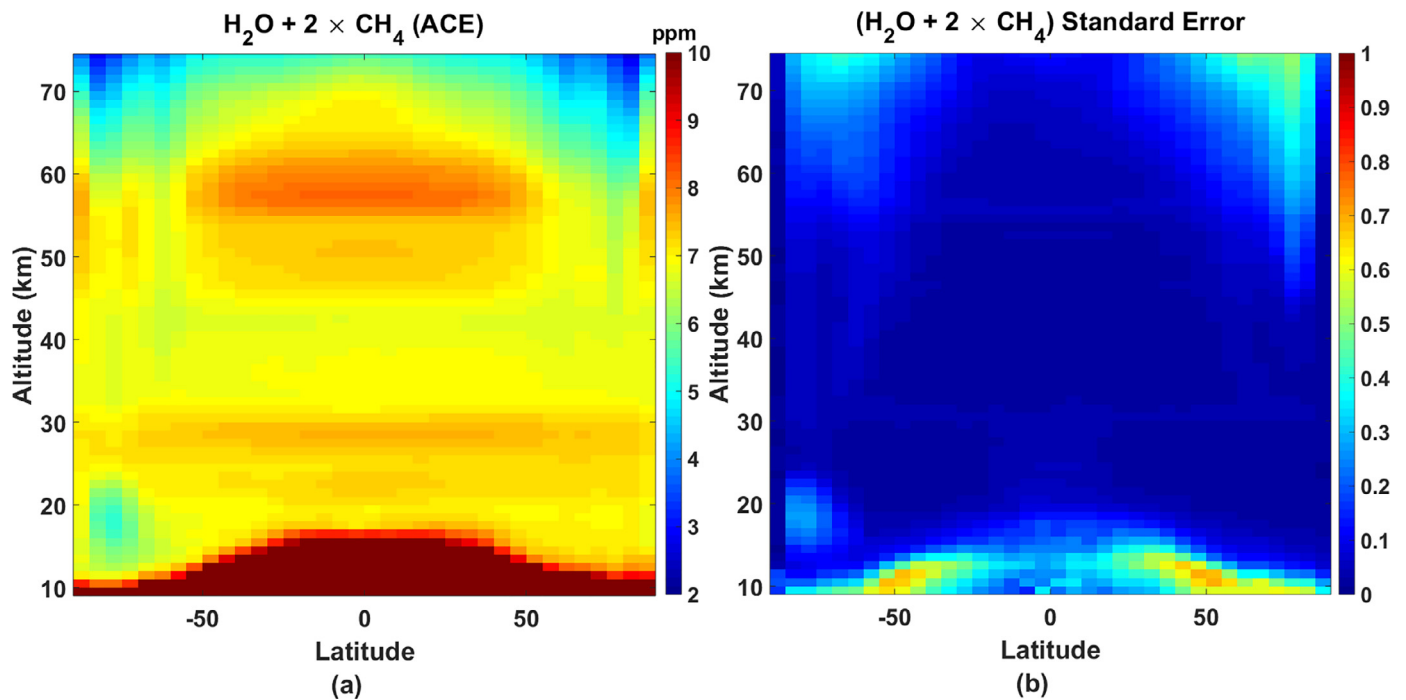
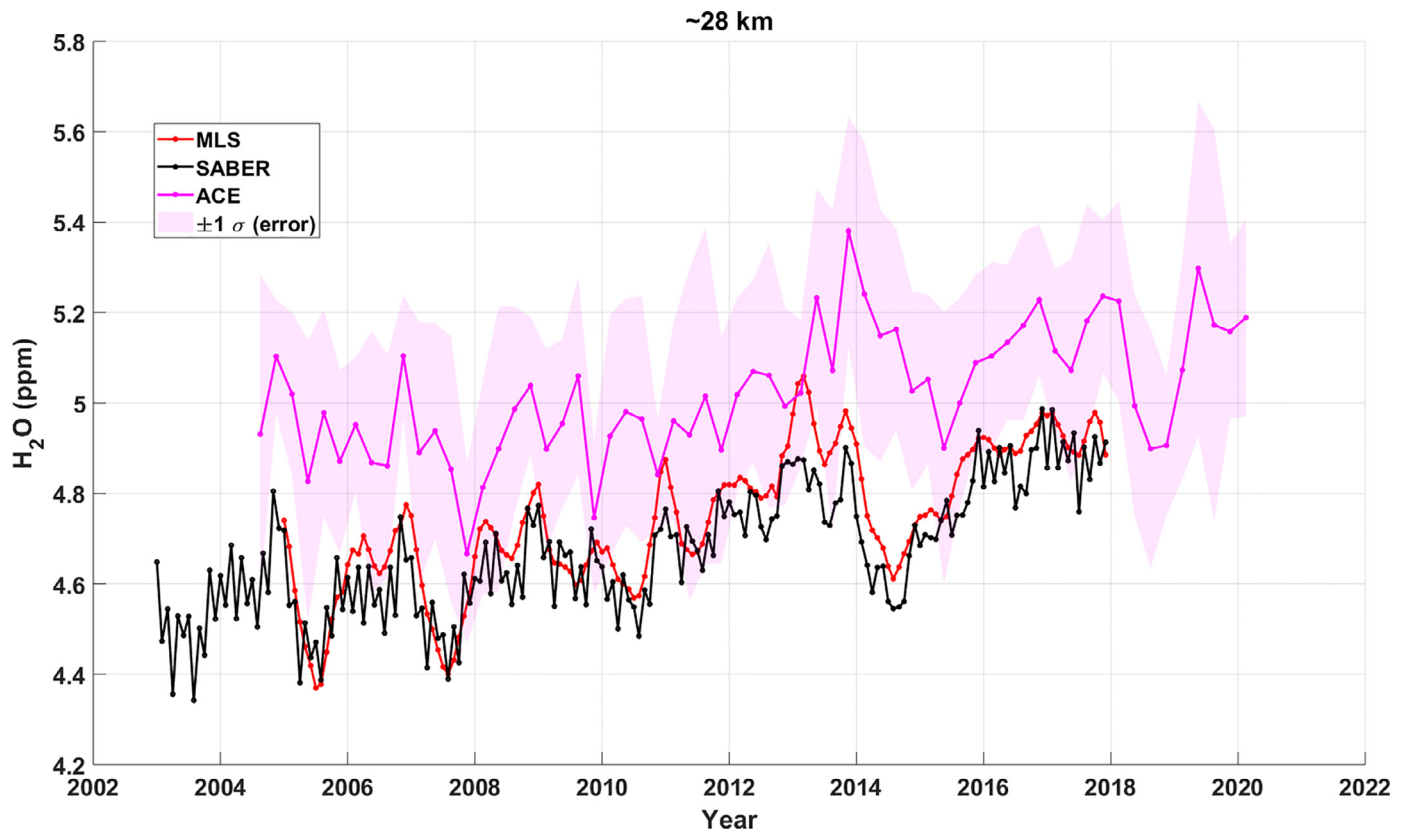
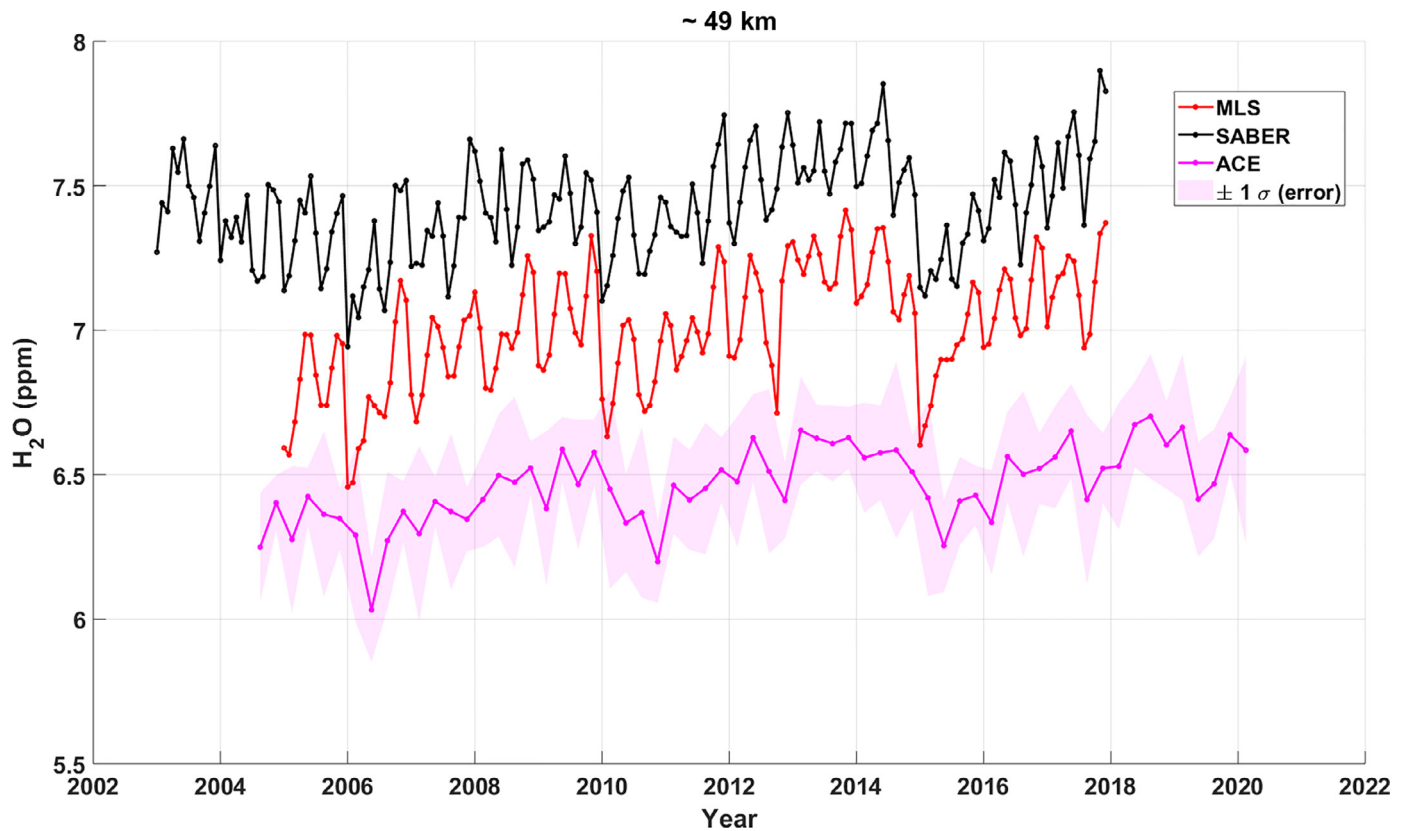


Fig. 3. ACE-FTS potential water a) average altitude-latitude distribution and b) relative standard error distribution.

~ 63 km and ~ 82 km ACE-FTS, MLS and SABER time series are generally in good agreement. It should be noted that occultation sounders such as ACE-FTS sample the atmosphere [11] very differently than emission sounders such as MLS and SABER so these comparisons should be interpreted with caution (see Fig. 11 in [11]). In particular, the relatively high ACE-FTS H₂O abundance at 28 km (Fig. 4) is explained using Fig. 1 which shows that the H₂O VMR increases with latitude. ACE's orbit [11] preferentially samples high latitudes, leading to the observed high bias. The low bias of ACE at 49 km (Fig. 5) is explained in a similar way because in

this case the H₂O VMR decreases with increasing latitude (Fig. 1), leading to a low bias. At higher altitudes, the H₂O abundances are more even at a given altitude and the agreement is better.

SABER linear trends and solar responses for 18 altitude levels (14.5 km - 96.7 km) for 2003–2017 [9] and MLS trends and solar responses for 36 altitude levels (14.7 km - 86 km) for 2005–2017 [9] are compared with ACE-FTS data. Linear trends and solar responses for altitude levels 14.5 km - 94.5 km for 2004 (JJA) - 2020 (DJF) were calculated for ACE-FTS data. The ACE H₂O VMRs of the first two quarters (2004 MAM and 2004 JJA) were removed

Fig. 4. ACE-FTS H_2O time series comparison at ~ 28 km with MLS and SABER data.Fig. 5. ACE-FTS H_2O time series comparison at ~ 49 km with MLS and SABER data.

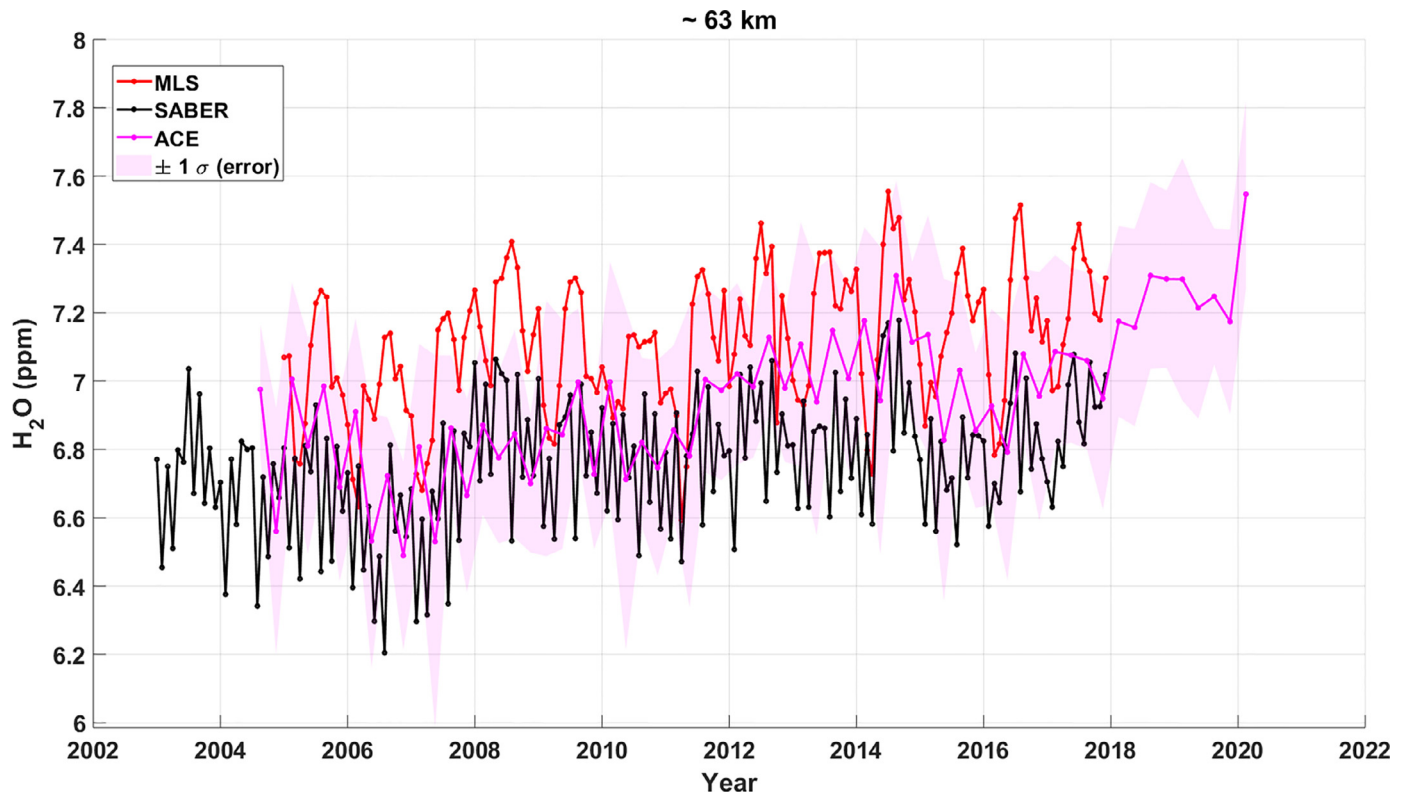


Fig. 6. ACE-FTS H₂O time series comparison at ~ 63 km with MLS and SABER data.

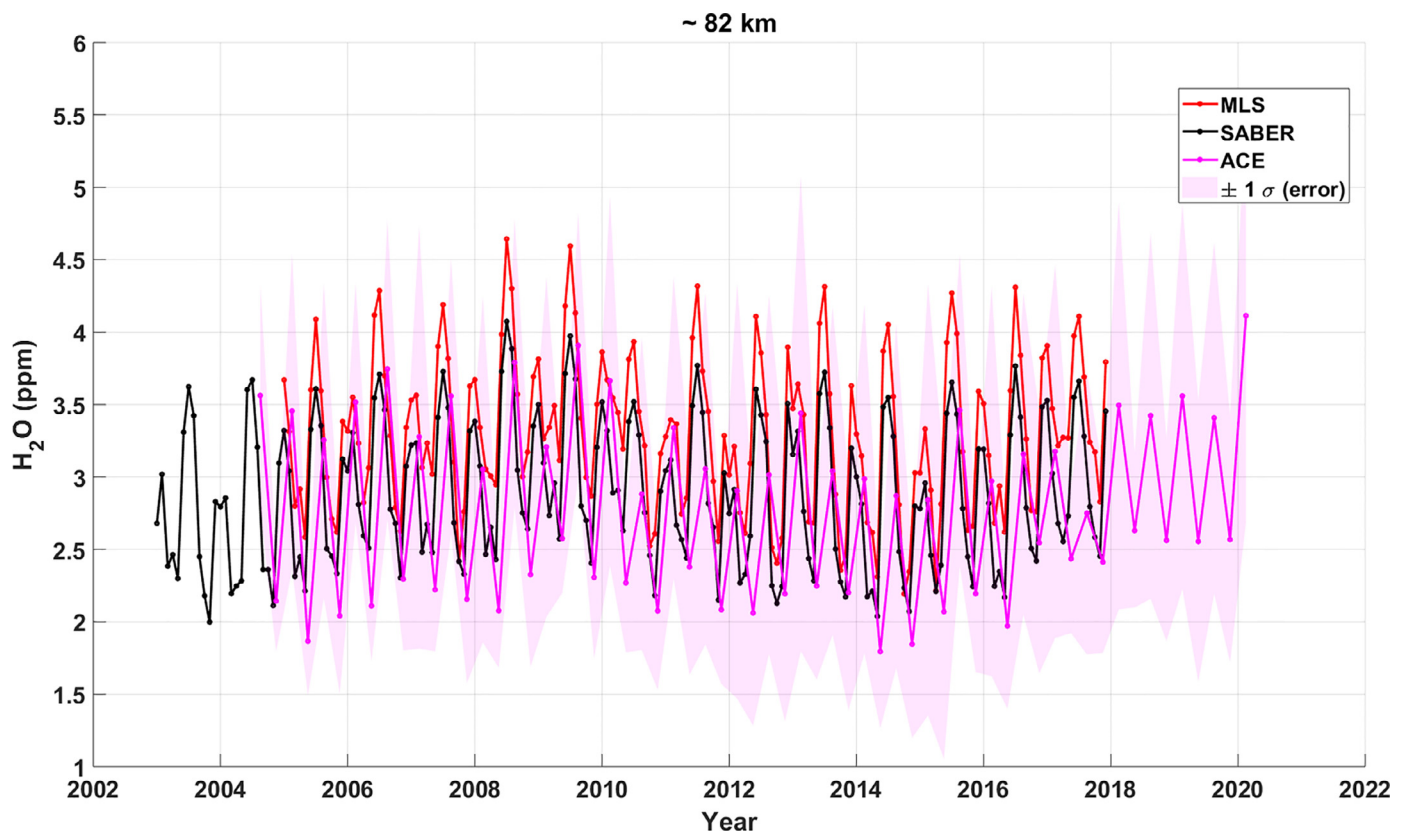


Fig. 7. ACE-FTS H₂O time series comparison at ~ 82 km with MLS and SABER data.

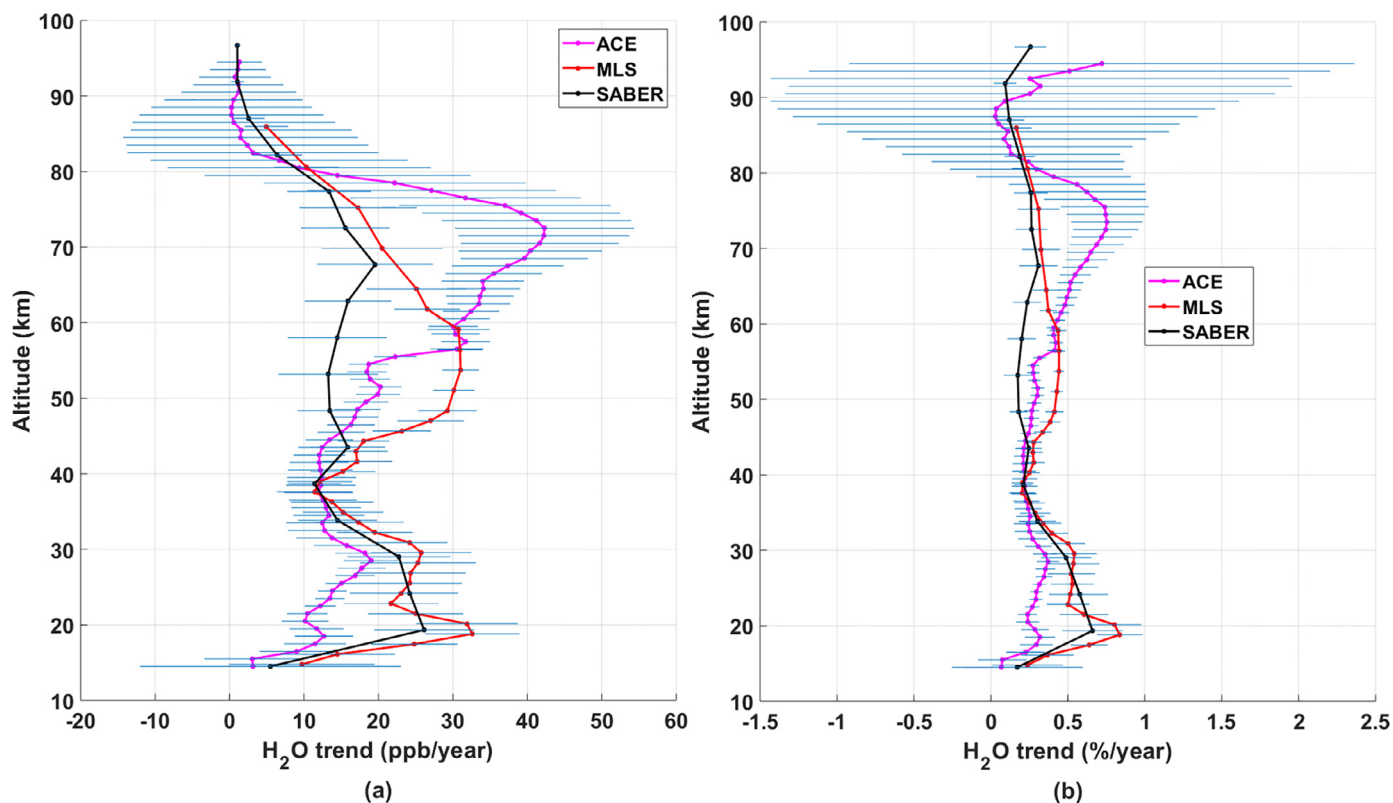


Fig. 8. ACE-FTS (55°S - 55°N) H₂O a) absolute trend and b) percentage trend comparison with MLS and SABER data (error bars are 1 σ).

from the trend analysis for all the altitudes (they show significantly higher values). Fig. 8 displays the linear trend values (ppb/year and percentage) for ACE-FTS, SABER and MLS and Fig. 9 shows the solar response for MLS, SABER and ACE data (with 1 standard deviation error bars). MLS and SABER linear trends and solar responses were calculated by Yue et al. [9] using multiple linear regression for the global mean H₂O times series for each altitude level. The annual and semi-annual oscillations, QBO and El Niño-Southern Oscillation terms were fitted for both MLS and SABER time series and removed [9]. The MLS and SABER times series have monthly points with each point calculated as a "bimonthly running mean". The ACE times series points are quarterly averages (DJF, MAM, JJA, SON).

ACE-FTS absolute and linear percentage trends and solar responses were calculated using linear regression for the quarterly time series for altitudes 14.5 km - 94.5 km and for the latitude region 55°S - 55°N. Note that the trends are probably not linear, but a linear model captures the general increase with time. The linear regression model consisted of a constant and terms for time, solar cycle response (F10.7 index), annual and semi-annual variations with phase terms (i.e., $\text{VMR H}_2\text{O}(t) = a + bt + c_1 \sin(2\pi t/4 + \phi_1) + c_2 \sin(\pi t/4 + \phi_2) + dF10.7$). The term b in the regression model (absolute trends) and the term d (solar responses) are plotted in Figs. 8a and 9a. Linear percentage trends and solar responses presented in Figs. 8b and 9b were obtained by dividing b and d by the average H₂O VMR for each altitude.

Absolute and percentage solar responses of ACE-FTS, MLS and SABER are in general agreement with each other, although at certain altitudes there are significant differences. MLS and SABER H₂O linear trends are in good agreement (15 - 25 ppb/year) between the altitudes of 14.5 km and 44.5 km, ACE-FTS trends are smaller (10 - 15 ppb/year). Between the altitudes of 40.5 km and 70.5 km, MLS values are ~ 30 ppb/year, ACE-FTS values vary between 15 ppb/year and 40 ppb/year and SABER values are ~ 15 ppb/year.

Above 70.5 km all trend values start to decrease and converge to 0 around 80 km.

Absolute and percentage linear trends and solar responses were also calculated for CH₄ (Figs. 10 and 11) and potential water (Figs. 12 and 13) using linear regression of the time series for altitudes 14.5 km - 74.5 km and for the latitude region 55°S - 55°N similar to ACE-FTS H₂O VMRs. Linear trends for CH₄ are quite variable; between the altitudes 14.5 km - 29.5 km ACE-FTS CH₄ trends fluctuate between 2 ppb/year - 8 ppb/year and from 29.5 km to 74.5 km trends start to decrease continuously from 4 ppb/year to 0.5 ppb/year (linear percentage trends of ACE-FTS CH₄ VMRs vary between 0.2 - 1.5%/year). SCIAMACHY solar occultation measurements also provide linear trends for CH₄ VMRs for the 2003-2011 time period and for 15 - 45 km [10]. Although SCIAMACHY and ACE-FTS linear trends profiles do not agree (ACE-FTS trend values larger by 2-3 ppb/year at each altitude) the shape of the trend profiles are similar (note that the time periods are different). Note that although the ACE trend values do not agree with SCIAMACHY values, the VMR profiles for both H₂O [10] and CH₄ [14] do agree. The solar responses for CH₄ VMRs are very small below 60 km (fluctuating between -0.04 ppm/100 sfu and +0.04 ppm/100 sfu). Above 60 km solar responses decrease and start reaching negative values (-0.02 ppm/100 sfu) around 70 km. Potential water linear trends (Figs. 12) and solar responses (Figs. 13) are very similar to H₂O trends and solar responses, because CH₄ contributions to the trends are relatively small.

The increasing CH₄ percentage trend with altitude in the stratosphere (Fig. 10b) is surprising. The potential water (Fig. 12b) does not show this trend and the CH₄ trend is an likely an artifact caused by a change in the conversion of CH₄ to H₂O. It seems that early in the mission a higher percentage of CH₄ converted to H₂O near the stratopause than later in the mission. This is based on Figs. 8, 10 and 12, in which older air in the upper stratosphere has

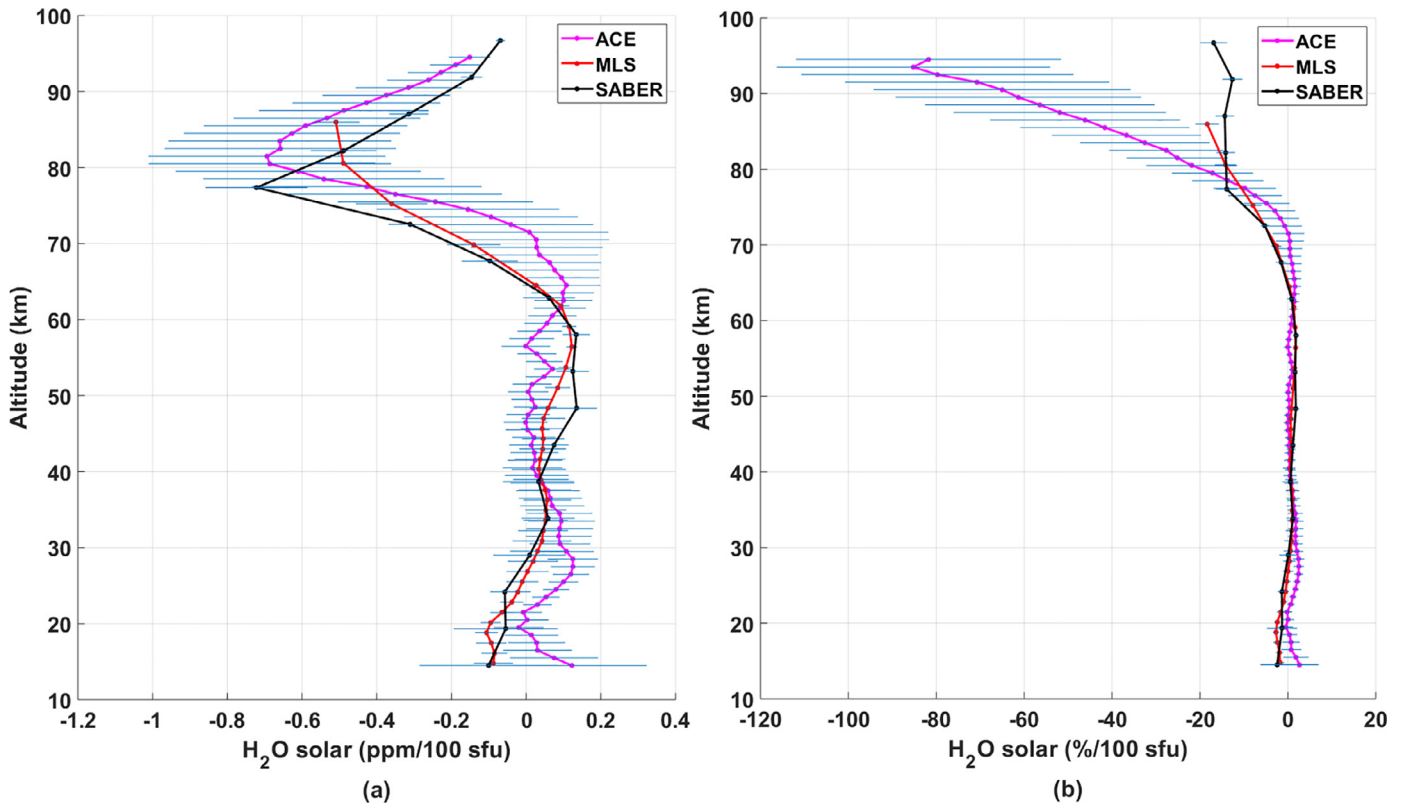


Fig. 9. ACE-FTS (55°S - 55°N) H₂O a) absolute and b) percentage solar response comparison with MLS and SABER data (error bars are 1 σ).

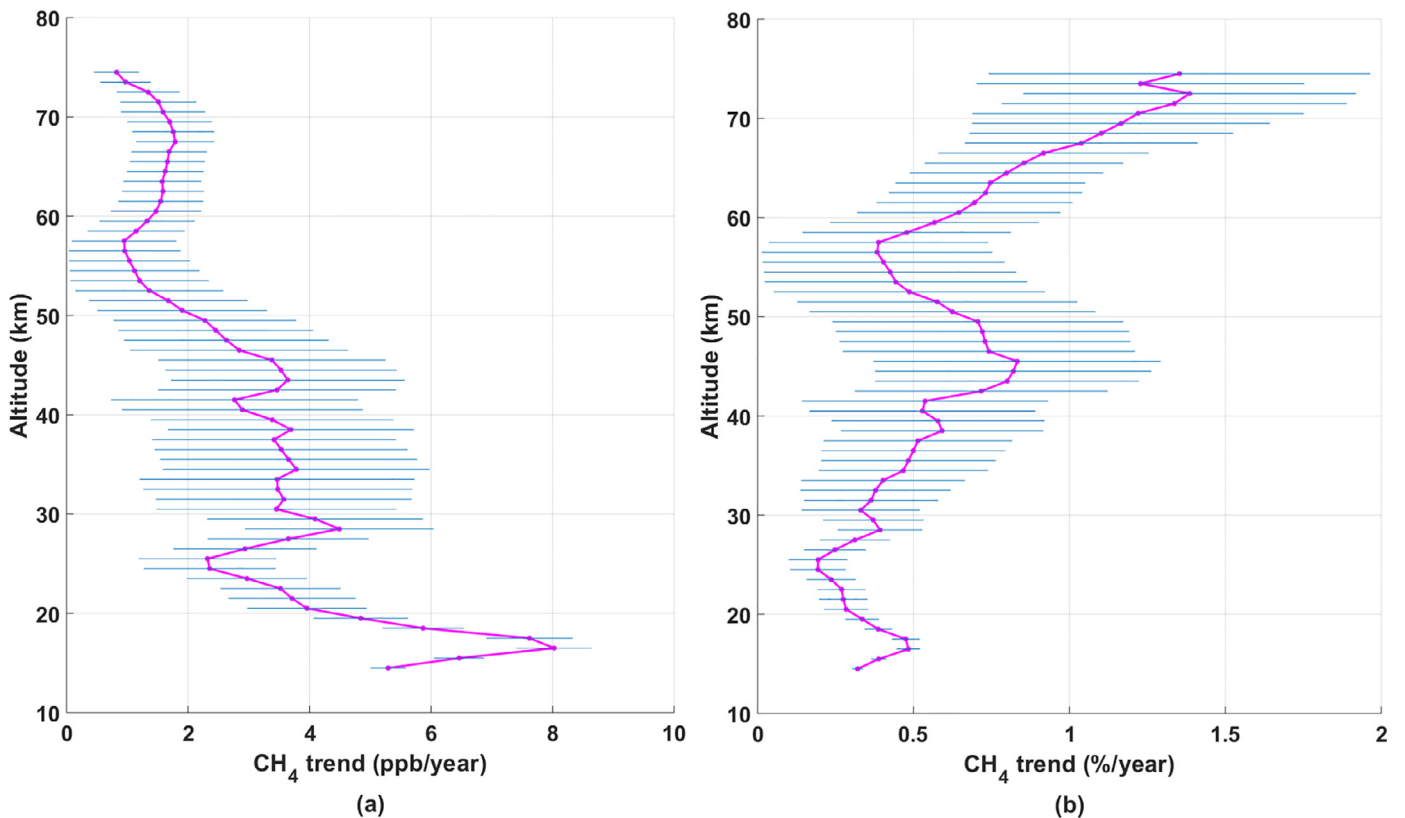


Fig. 10. ACE-FTS (55°S - 55°N) CH₄ a) absolute trend and b) percentage trend (error bars are 1 σ).

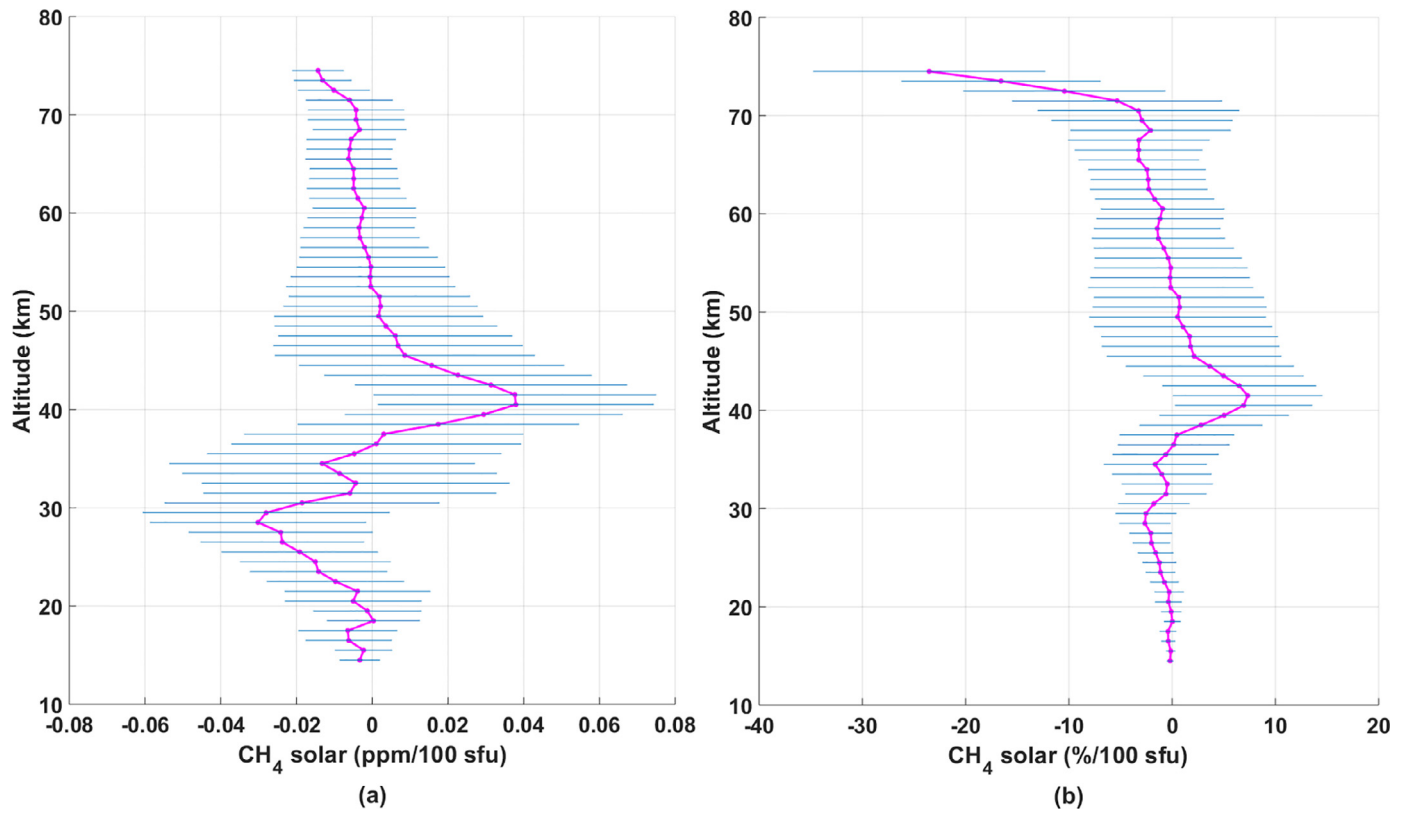


Fig. 11. ACE-FTS (55°S - 55°N) CH₄ a) absolute and b) percentage solar response (error bars are 1 σ).

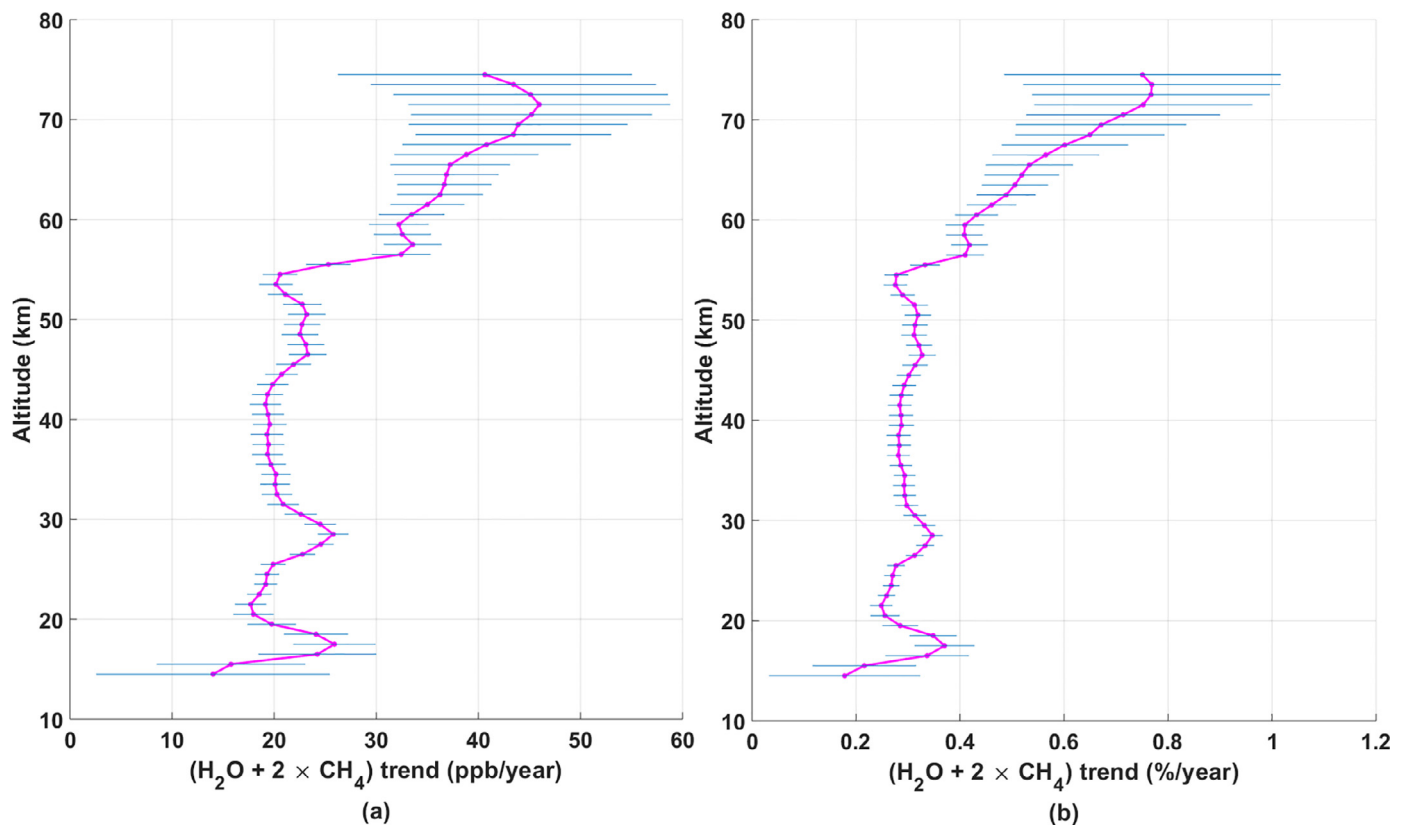


Fig. 12. ACE-FTS (55°S - 55°N) potential water a) absolute trend and b) percentage trend (error bars are 1 σ).

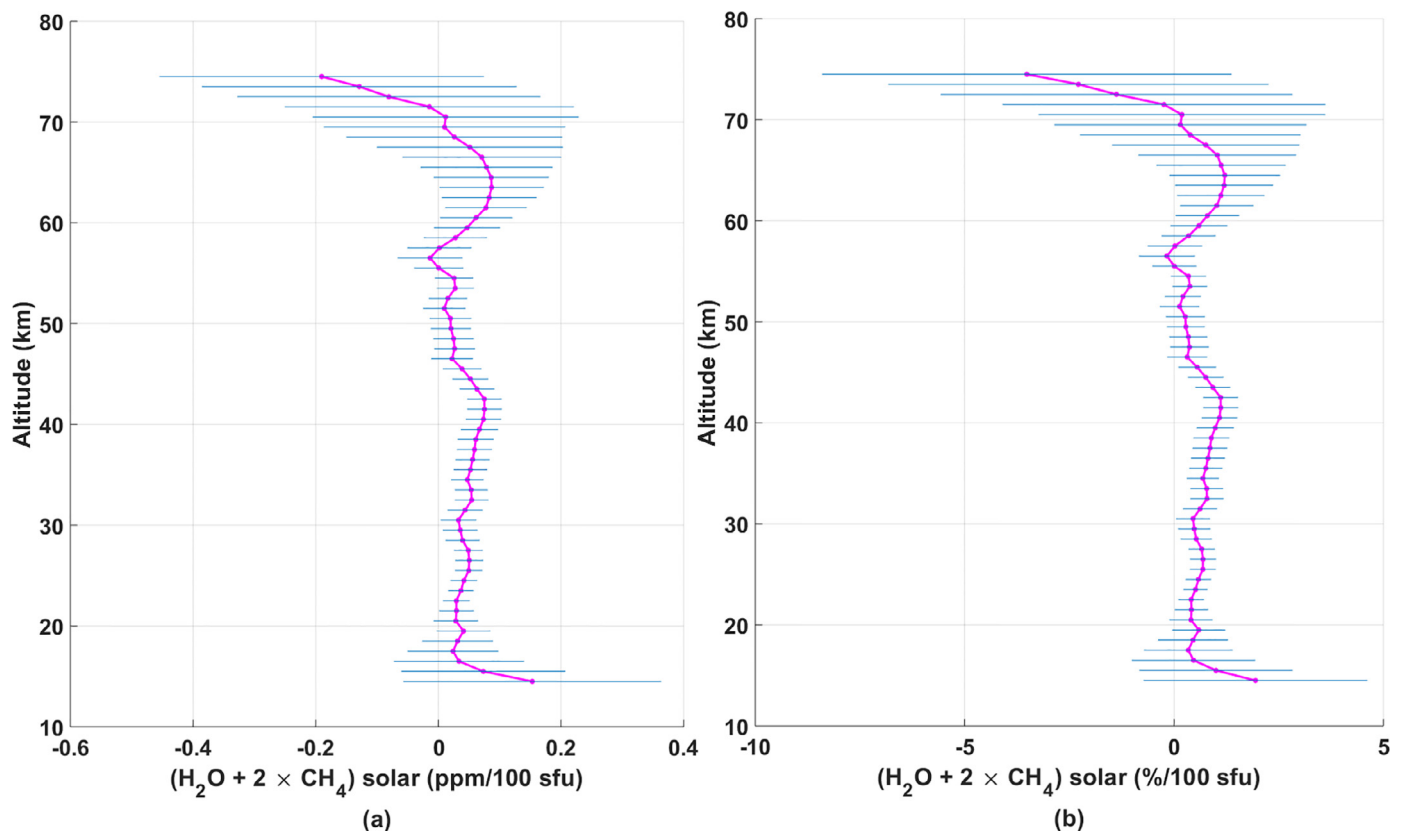


Fig. 13. ACE-FTS (55°S - 55°N) potential water a) absolute and b) percentage solar response (error bars are 1σ).

a larger CH_4 trend, H_2O has a smaller trend, while potential water shows no change in trend with altitude.

ACE trends cannot be attributed to drifts in measurements. The latest processing versions (v.4.0 and v.4.1) have very little drift as demonstrated by the good agreement between ACE trends for many tropospheric molecules with trends from accurate NOAA flask data [15].

Between 50 km and 75 km, CH_4 trends are less than 1 ppb/year and H_2O trends are above 20 ppb/year. At all altitudes (10 km to 75 km) methane oxidation does not explain the water vapor trends (Fig. 8a). Therefore, the observed ACE-FTS H_2O trends (above 10 km) should be mainly attributed to H_2O transport from the troposphere and to atmospheric dynamics. SABER and MLS H_2O observations also lead to the same conclusion [9]. The major factor controlling the transport of H_2O across the tropical tropopause is the cold point temperature, along with upward transport by the Brewer-Dobson circulation. However, overshooting convection across the tropopause and small-scale wave activity also contribute [16].

Solar response of ACE-FTS H_2O agrees with SABER and MLS values (Fig. 9). At higher altitudes (above 70 km) ACE-FTS, SABER and MLS data show increasingly negative solar responses and below 70 km small positive responses.

4. Conclusion

Absolute and percentage linear trends and solar responses of ACE-FTS, MLS and SABER H_2O are in general agreement with each other. Potential water linear trends and solar responses are very similar to H_2O trends and solar responses, because the CH_4 contribution to the trends is relatively small. At all altitudes (10 km to 75 km) methane oxidation does not explain the water vapor trends and ACE-FTS H_2O trends (above 10 km) should be mainly

attributed to H_2O transport from the troposphere and to atmospheric dynamics.

Declaration of Competing Interest

We know of no conflicts of interest associated with this publication.

CRediT authorship contribution statement

Anton M. Fernando: Formal analysis, Writing - original draft. **Peter F. Bernath:** Conceptualization, Supervision, Writing - review & editing. **Christopher D. Boone:** Data curation, Writing - review & editing.

Acknowledgements

The ACE mission is supported by the Canadian Space Agency (9F045-180032/001/MTB). We thank J. Yue and Q. Gan for providing the MLS and SABER data plotted in Figs. 4–9.

Supplementary material

Supplementary material associated with this article can be found, in the online version, at doi:10.1016/j.jqsrt.2020.107268.

References

- [1] Solomon S, Rosenlof KH, Portmann RW, Daniel JS, Davis SM, Sanford TJ, et al. Contributions of stratospheric water vapor to decadal changes in the rate of global warming. *Proc Natl Acad Sci* 2010;327(5970):1219–23.
- [2] Dessler AE, Schoeberl MR, Wang T, Davis SM, Rosenlof KH. Stratospheric water vapor feedback. *Proc Natl Acad Sci* 2013;110(45):18087–91.
- [3] Solomon S. Stratospheric ozone depletion: a review of concepts and history. *Rev Geophys* 1999;37(3):275–316.

- [4] Jones SC, Bernath PF, Boone CD. Properties of polar mesospheric clouds from ACE satellite infrared spectra. *J Quant Spectrosc Radiat Transf* 2019;238:106518.
- [5] Zhao XR, Sheng Z, Shi HQ, Weng LB, Liao QX. Long-term trends and solar responses of the mesopause temperatures observed by SABER during the 2002–2019 period. *Journal of Geophysical Research: Atmospheres* 2020;125. e2020JD032418
- [6] Lübken F-J, Berger U, Baumgarten G. On the anthropogenic impact on long-term evolution of noctilucent clouds. *Geophys Res Lett* 2018;45(13):6681–9.
- [7] Finlayson-Pitts B, Pitts J. *Chemistry of upper and lower atmosphere*. San Diego, CA: Academic Press; 2000.
- [8] Nassar R, Bernath PF, Boone CD, Manney GL, McLeod SD, Rinsland CP, et al. Stratospheric abundances of water and methane based on ACE-FTS measurements. *Geophys Res Lett* 2005;32:L15S04.
- [9] Yue J, Russell III J, Gan Q, Wang T, Rong P, Garcia R, et al. Increasing water vapor in the stratosphere and mesosphere after 2002. *Geophys Res Lett* 2019;46(22):13452–60.
- [10] Noël S, Weigel K, Bramstedt K, Rozanov A, Weber M, Bovensmann H, et al. Water vapour and methane coupling in the stratosphere observed using SCIAMACHY solar occultation measurements. *Atmos Chem Phys* 2018;18(7):4463–76.
- [11] Bernath P. The Atmospheric Chemistry Experiment (ACE). *J Quant Spectrosc Radiat Transf* 2017;186:3–16.
- [12] Boone C, Bernath P, Cok D, Jones S, Steffen J. Version 4 retrievals for the atmospheric chemistry experiment fourier transform spectrometer (ACE-FTS) and imagers. *J Quant Spectrosc Radiat Transf* 2020;247:106939.
- [13] Gordon I, Rothman L, Hill C, Kochanov R, Tan Y, Bernath P, et al. The HITRAN2016 molecular spectroscopic database. *J Quant Spectrosc Radiat Transf* 2017;203:3–69.
- [14] Noël S, Bramstedt K, Hilker M, Liebing P, Plieninger J, Reuter M, et al. Stratospheric CH₄ and CO₂ profiles derived from SCIAMACHY solar occultation measurements. *Atmos Meas Tech* 2016;9(4):1485–503.
- [15] Bernath PF, Crouse J, Hughes RC, Boone CD. The Atmospheric Chemistry Experiment Fourier Transform Spectrometer (ACE-FTS) version 4.1 retrievals: trends and seasonal distributions. *Journal of Quantitative Spectroscopy and Radiative Transfer* 2020. Submitted
- [16] Randel W, Park M. Diagnosing observed stratospheric water vapor relationships to the cold point tropical tropopause. *J Geophys Res* 2019;124(13):7018–33.